PHILOSOPHICAL TRANSACTIONS OF THE ROYAL SOCIETY A MATHEMATICAL, PHYSICAL & ENGINEERING SCIENCES

Pulsar Timing and Relativistic Gravity

J. H. Taylor

Phil. Trans. R. Soc. Lond. A 1992 **341**, 117-134
doi: 10.1098/rsta.1992.0088

Pulsar timing and relativistic gravity

By J. H. Taylor

Joseph Henry Laboratories and Physics Department, Princeton University, Princeton, New Jersey 08544, U.S.A.

In addition to being fascinating objects to study in their own right, pulsars are exquisite tools for probing a variety of issues in basic physics. Recycled pulsars, thought to have been spun up in previous episodes of mass accretion from orbiting companion stars, are especially well suited for such applications. They are extraordinarily stable clocks, approaching and perhaps exceeding the long-term stabilities of the best terrestrial time standards. Most of them are found in binary systems, with orbital velocities as large as $10^{-3}\,c$. They provide unique opportunities for measuring neutron star masses, thereby yielding fundamental astrophysical data difficult to acquire by any other means. And they open the way for high precision tests of the nature of gravity under conditions much more 'relativistic' than found anywhere within the Solar System. Among other results, pulsar timing observations have convincingly established the existence of quadrupolar gravitational waves propagating at the speed of light. They have also placed interesting limits on possible departures of the strong-field nature of gravity from general relativity, on the rate of change of Newton's constant, G, and on the energy density of low-frequency gravitational waves in the universe.

1. Introduction and background

Those of us who were not in Cambridge a quarter century ago can only guess at the utter astonishment that Hewish, Bell, and colleagues must have felt as the potential significance of their remarkable discovery unfolded (Hewish *et al.* 1968). A great many of the observable characteristics of pulsars were unexpected, but none more so than the extraordinary regularity of their timing behaviour. Early measurements showed that pulsars have fractional timing instabilities (after removal of a fixed slowdown rate) no larger than 10^{-10} over many months, and it turns out that such figures were but hints of better things to come. The fractional instabilities of some pulsars have now been shown to lie in the 10^{-14} range, or better, over timescales of many years. Pulsars thus appear to be nature's most stable clocks, and as such, they provide a cornucopia of challenges and opportunities for the ambitious observer. Pulsar timing has become an important subfield of observational radio astronomy, and a significant new tool in experimental physics as well. Its interesting consequences have spread through many areas of research including fundamental astrometry, stellar evolution, cosmology, gravitation physics, and time-keeping metrology.

In this paper I describe and review the current status of high-precision pulsar timing experiments, especially emphasizing their intricate connections with relativistic gravity. I also discuss some desirable (and plausibly attainable) goals for pulsar timing experiments in the future. I argue that carefully documented efforts extending over several decades could lead to important new results in cosmology and

Phil. Trans R. Soc. Lond. A (1992) **341**, 117–134
Printed in Great Britain

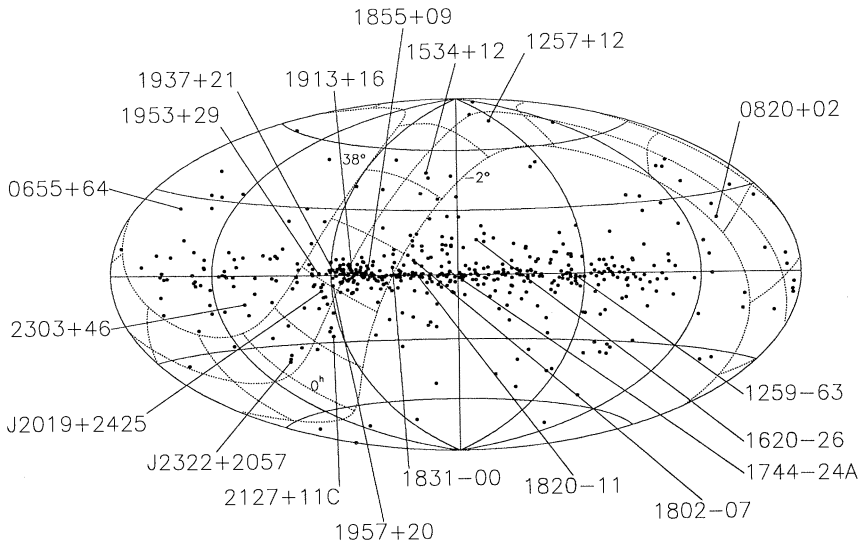

Figure 1. The distribution of 553 known pulsars in galactic coordinates. Longitude increases toward the left, with $l = 0$, $b = 0$ at the centre. Sky coverage of the Arecibo Observatory's 305 m radio telescope is illustrated with dotted lines at celestial declinations $\delta = -2°$, 18°, 38°, and right ascensions $\alpha = 0^h, 2^h, \ldots, 22^h$. Pulsar names prefixed with 'J' are given in J2000 coordinates; the remainder use the older, B1950 convention.

fundamental physics, results that are not presently achievable by any other known techniques.

For the topics treated here, the most rewarding pulsars to study are those that have been 'recycled' through a process of mass exchange in an evolving binary star system (see Alpar *et al.* 1982; Bhattacharya & van den Heuvel 1991, and references therein). Like all radio pulsars, these objects are believed to be rapidly spinning, strongly magnetized neutron stars whose energetics are dominated by their spindown luminosities. Their evolution has been significantly modified by an accretion episode in which mass and angular momentum were transferred from an orbiting companion star. Recycled pulsars make up a small fraction of the total, and most of them are still members of gravitationally bound binary systems. They are generally much older, spin faster, and have smaller magnetic fields than ordinary pulsars. For these reasons they are also the most precisely 'timetable', and intrinsically the most predictable as clocks. They are the class of pulsars best suited for detecting, using, and testing the effects of relativistic gravity.

As I write these words in March 1992, the working list of pulsar parameters that we keep in Princeton contains 553 pulsars. Their distribution in galactic coordinates is illustrated by the map in figure 1. Nearly 50 are recycled objects, but two-thirds of these are located in globular star clusters whose gravitationally complicated environments and large distances from the Sun make them less interesting for high-precision timing experiments. There still remain, however, a sizeable number of attractive candidates for precise timing. Nineteen individual pulsars that will be mentioned in this paper are identified by name in figure 1. Nearly all of these are in the recycled class. Note that 12 of the 19 lie at declinations between $-2°$ and $+38°$, the range of sky accessible to the 305 m telescope of the Arecibo Observatory. All but two of these objects (PSRs 0820+02 and 1831−00) were in fact discovered at

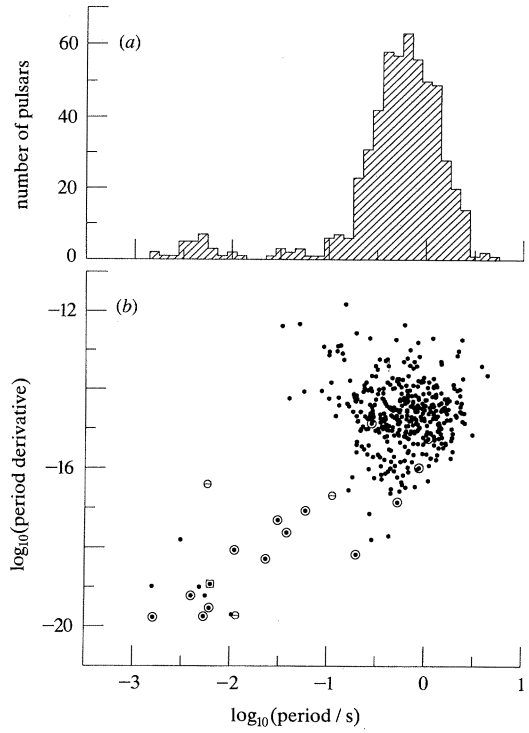

Figure 2. (*a*) Histogram showing the period distribution of 553 pulsars. (*b*) Periods and period derivatives of 433 pulsars. Binary pulsars are shown as encircled dots, while PSR 1257 + 12, which has planetary-size companions, has a square surrounding its symbol. Three pulsars with negative measured derivatives are plotted (as absolute values) with the symbol '⊖'. Note that many recently discovered short-period pulsars, especially the relatively weak objects found in globular clusters, do not yet have measured derivatives.

Arecibo: the uniquely high sensitivity of this instrument is crucially important for pulsar searches, as well as timing experiments, and a large fraction of high precision pulsar timing work has been done with its benefit.

The period distribution of known pulsars is illustrated at the top of figure 2. This bimodal histogram strongly suggests the need to invoke two classes of pulsars, and indeed most of the objects with $P \lesssim 0.1$ s belong in the recycled category. Membership of a pulsar in the recycled group can be determined more reliably from the two-dimensional plot at the bottom of figure 2, which includes all 433 pulsars with known period derivatives, $\dot{P}$. Most of the recycled pulsars have both short periods and small period derivatives, and are thus found in the lower left-hand portion of the $P, \dot{P}$ diagram. They have spin-down time scales $P/\dot{P} > 10^8$ years, and to the best of our current understanding they may remain active pulsars for times comparable to the Hubble time, or even longer.

2. Fundamentals of pulsar timing

(*a*) *Measuring* TOAs

Measurements of pulse times of arrival (TOAs) are invariably carried out by synchronously averaging the received signal to yield an integrated profile, effectively a cross section through the angular power pattern of the spinning pulsar's radio

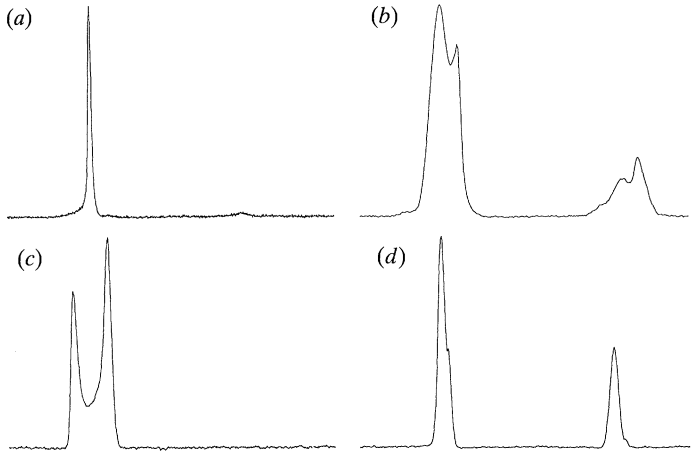

Figure 3. Average profiles of four pulsars timed regularly at the Arecibo Observatory. The observations were made at frequencies near 1400 MHz, with integration times of several hours. (*a*) 1534+12, 37.9 ms; (*b*) 1855+09, 5.4 ms; (*c*) 1913+16, 59.0 ms; (*d*) 1937+21, 1.6 ms.

beam. To reduce the necessary data rate by many order of magnitude, the averaging is usually done in real time by using special-purpose digital hardware (Stinebring *et al.* 1992). After square-law detection, the signal is sampled an integral number of times (typically 1024) per topocentric pulsar period. Accumulated average profiles are recorded every few minutes, together with accurate time information derived from the observatory's time and frequency standard. Figure 3 shows examples of the average profiles of four pulsars being times regularly at Arecibo, in these cases integrated over several hours.

Experience shows that to a good approximation, recorded profiles for a given pulsar at a particular observing frequency are identical except for a DC bias, a multiplicative scale factor, a shift of time origin, and additive random noise. In other words, each observed profile $p(t)$ can be related to a corresponding 'standard profile', $s(t)$, by an equation of the form

$$p(t) = a + bs(t-\tau) + g(t), \tag{1}$$

where a, b, and τ are constants, $g(t)$ is a random variable representing radiometer and background noise, and $0 \leqslant t \leqslant P$ where P is the topocentric period. In common practice the profiles are discretely sampled at times $t_j \equiv j\Delta t$, with $\Delta t = P/N$ for some integer N. The problem of measuring TOAs amounts to determining the time shift τ as accurately as possible and adding it to the recorded start time of the observation. The Appendix describes our favoured procedure for doing this.

(*b*) *The timing model*

An extensive theoretical framework for analysing pulsar timing data has been developed over the years (Manchester & Taylor 1977; Damour & Deruelle 1986; Taylor & Weisberg 1989; Ryba & Taylor 1991; Damour & Taylor 1992, and references therein). Since the observations are necessarily carried out from a moving observatory, analysis of a series of measured TOAs must begin with an accurate model of Solar System dynamics. Binary pulsars of course have orbital motions of their own, further complicating the analysis procedure; in compensation, however, they

provide opportunities to acquire a wealth of additional information beyond that available from single pulsars.

To extract the maximum possible information from pulsar timing observations, one begins by transforming each measured topocentric TOA, say $t_{\rm obs}$, to a corresponding proper time of emission, say T, in the pulsar frame. Under the assumption of a simple deterministic spin-down law, the rotational phase of the pulsar is related to T according to

$$\varphi(T) = \nu T + \tfrac{1}{2}\dot{\nu}T^2 + \tfrac{1}{6}\ddot{\nu}T^3, \tag{2}$$

where ν is the rotation frequency and the phase is measured in cycles. The transformation from terrestrial time to pulsar proper time must be done relativistically, in accord with the weak-field, slow-motion limit of general relativity. (To sufficient accuracy, other viable relativistic theories of gravity would yield equivalent results in this limit.) The necessary equations include terms related to positions, velocities, and masses within the solar system, and to propagation effects in the interstellar medium. For binary pulsars there will also be terms representing the consequences of orbital motion. The orbital effects have been worked out in a very general way by Damour & Deruelle (1985, 1986).

With presently achievable accuracies, all significant terms in the time transformation can be summarized in the single equation

$$\begin{aligned} T = {} & t_{\rm obs} - t_0 + \Delta_{\rm C} - D/f^2 + \Delta_{\rm R\odot}(\alpha, \delta, \mu_\alpha, \mu_\delta, \pi) + \Delta_{\rm E\odot} - \Delta_{\rm S\odot}(\alpha, \delta) \\ & - \Delta_{\rm R}(x, e, P_{\rm b}, T_0, \omega, \dot{\omega}, \dot{P}_{\rm b}, \dot{x}, \dot{e}, \delta_\theta) - \Delta_{\rm E}(\gamma) - \Delta_{\rm S}(r, s) - \Delta_{\rm A}. \end{aligned} \tag{3}$$

Here t_0 is a nominal equivalent TOA at the solar system barycenter; $\Delta_{\rm C}$ represents any measured offsets between the local observatory clock and the best terrestrial standard of time; D/f^2 is the dispersive delay for propagation at frequency f over the path from pulsar to Earth; $\Delta_{\rm R\odot}, \Delta_{\rm E\odot}$, and $\Delta_{\rm S\odot}$ are propagation delays and relativistic time adjustments within the Solar System; and $\Delta_{\rm R}, \Delta_{\rm E}, \Delta_{\rm S}$, and $\Delta_{\rm A}$ are similar terms for a binary pulsar's orbit. Subscripts on the various Δs indicate the nature of the delays, which include 'Roemer', 'Einstein', and 'Shapiro' effects within the Solar System, and these as well as 'Aberration' effects in the pulsar orbit. Note that the Roemer terms have amplitudes roughly equal to the orbital periods times v/c, where v is the orbital velocity and c the speed of light. The Einstein terms are proportional to v^2/c^2, multiplied by the orbital eccentricities. The Shapiro delay in the Solar System has a maximum value of *ca.* 120 μs when the line of sight grazes the limb of the Sun, and depends logarithmically on the impact parameter. The corresponding delay within the binary orbit depends on the companion star's mass, the orbital phase, and the inclination i between the plane of the orbit and the plane of the sky. Full details on all of the terms in (3) can be found in the references quoted at the beginning of this subsection.

Equations (2) and (3) have been written to show explicitly the most significant dependences of pulsar phase on the set of potentially measurable pulsar parameters. In addition to the rotational frequency ν and its time derivatives, these parameters include the reference arrival time t_0, dispersion constant D, celestial coordinates α and δ, proper motion terms μ_α and μ_δ, and parallax π. For binary pulsars, as many as 13 orbital parameters can be measured as well. These include five that would be significant even in a purely keplerian analysis of orbital motion: the projected semi-major axis $x \equiv a_1 \sin i/c$, eccentricity e, binary period $P_{\rm b}$, longitude of periastron ω, and time of periastron T_0. If the experimental timing precision is high enough,

relativistic effects can yield up to eight 'post-keplerian' measurables: the secular derivatives $\dot{\omega}$, $\dot{P}_b$, $\dot{x}$, and $\dot{e}$, the Einstein parameter γ, the range and shape of the orbital Shapiro delay, r and s, and an orbital shape correction, δ_θ (see Damour & Taylor 1992, and references therein).

Parameter values are extracted from a set of TOAs by calculating the pulsar phases $\varphi(T)$ from (2) and minimizing the weighted sum of squared residuals,

$$\chi^2 = \sum_{i=1}^{M} \left(\frac{\varphi(T_i) - n_i}{\sigma_i / P} \right)^2, \tag{4}$$

with respect to each parameter to be determined. In this equation, n_i is the closest integer to $\varphi(T_i)$, and σ_i is the estimated uncertainty of the ith TOA (see Appendix). In the analysis of a given set of data, some parameters will be more readily measurable than others. When TOAs have been measured over many dates spread over several months, it generally follows that at least the celestial coordinates, spin parameters, and keplerian orbital elements will be measurable to many significant digits. The post-keplerian parameters are more challenging, however; an extensive analysis of their measurabilities in practical circumstances has been carried out recently by Damour & Taylor (1992).

(c) *Limits to attainable precision*

The information content of pulsar timing observations depends critically on the accuracy of the measured TOAs. Good experiment design therefore concentrates on choosing observing parameters so as to optimize the overall error budget for each observed pulsar. Raw statistical uncertainties can be estimated in the process of fitting observed profiles to standard profiles, as outlined in the Appendix. We find, for example, that the four pulsars whose profiles are illustrated in figure 3 yield measurement uncertainties of approximately 3, 3, 15, and 0.8 μs in five-minute observations with the Arecibo telescope at 1400 MHz. To these statistical errors one must add any systematic contributions from other sources such as clock offsets, uncompensated changes in interstellar propagation, errors in determining the effective frequencies of receiver passbands, and so on.

Recycled pulsars are inherently good enough clocks that reasonable estimates of the magnitudes of timing errors can be obtained by careful study of post-fit residuals. The two longest and most accurate sequences of pulsar timing observations now available are those obtained for PSRs 1937+21 and 1855+09 at the Arecibo Observatory. They began in late 1984 and early 1986, respectively, and observations have been made approximately biweekly over most of this time. Subsets of the data have been analysed and published several times in the past (Rawley *et al.* 1987, 1988; Stinebring *et al.* 1990; Ryba & Taylor 1991; Taylor 1991). Plots of the residuals through early 1992 are presented in figure 4. PSR 1937+21 is a single pulsar, and the timing model fitted to its data includes just nine parameters: $t_0, \nu, \dot{\nu}, D, \alpha, \delta, \mu_\alpha, \mu_\delta$, and π. PSR 1855+09, on the other hand, is a binary pulsar with orbital period $P_b \approx 12.3$ d. Its model includes the same nine quantities plus five keplerian and two post-keplerian orbital parameters, namely $x, e, P_b, T_0, \omega, r$, and s.

The very small post-fit timing residuals for PSRs 1937+21 and 1855+09 show that the fitted models account for nearly all of the observed timing behaviour. Indeed, at the present level of accuracy for PSR 1855+09 (the median uncertainty for the data illustrated is $\sigma = 0.86$ μs), the model provides an almost perfect fit. For PSR 1937+21 the median uncertainty is considerably smaller ($\sigma = 0.39$ μs before 1989.0

PHILOSOPHICAL TRANSACTIONS OF THE ROYAL SOCIETY A MATHEMATICAL, PHYSICAL & ENGINEERING SCIENCES

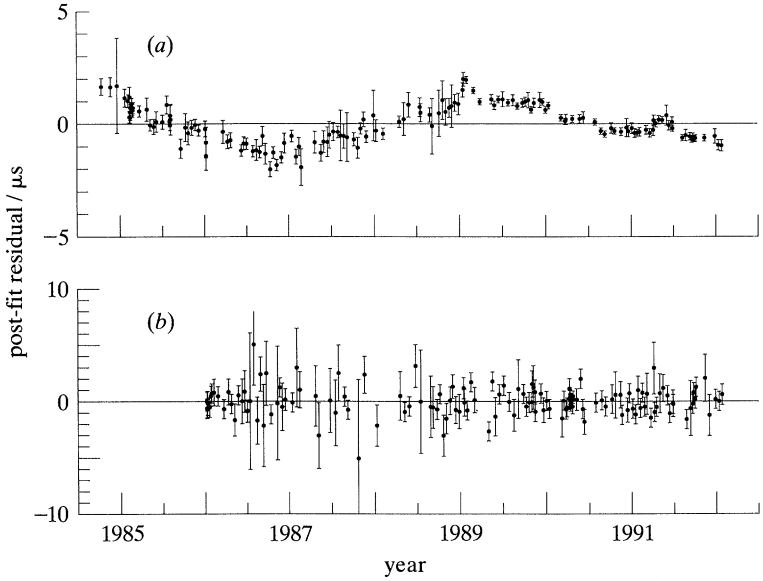

Figure 4. Post-fit timing residuals for (*a*) PSR 1937+21 and (*b*) PSR 1855+09, plotted as a function of date. Error bars correspond to estimated uncertainties in the TOAs; the reference atomic timescale is UTC(PTB). (Observations carried out in collaboration with L. Rawley, M. Davis, M. Ryba, and V. Kaspi.)

and $\sigma = 0.19$ μs thereafter), and systematic trends are seen in the residuals at levels $\lesssim 2$ μs. We have not yet conclusively identified the dominant sources of noise responsible for these trends. Some likely prospects include instabilities in the reference time standards, uncompensated changes in the propagation medium, errors in Solar System ephemerides, rotational instabilities in the pulsars, and a cosmic background of low-frequency gravitational waves (Bertotti *et al.* 1983; Blandford *et al.* 1984; Stinebring *et al.* 1990). The first three of these potential noise sources appear to have amplitudes corresponding to fractional instabilities $\sigma_z \approx 10^{-14}$ over time intervals up to five years, and the remaining noise sources are probably even smaller (Taylor 1991). These results have been used to provide significant limits on the energy density of a cosmic background of gravitational radiation (Stinebring *et al.* 1990; Ryba 1991). The data also imply that the limiting accuracy of pulsar timing measurements with present techniques is a few microseconds, or less, over many years.

3. Timing binary pulsars

(*a*) *The newtonian limit*

Twenty-one pulsars in orbiting systems have now been studied well enough to determine at least their basic parameters. Their names, periods, period derivatives, and orbital elements P_b, e, and x are listed in table 1. For each pulsar the orbital period P_b and projected semi-major axis x can be combined to give the mass function,

$$f_1(m_1, m_2, s) = \frac{(m_2 s)^3}{(m_1 + m_2)^2} = \frac{x^3}{(P_b/2\pi)^2}\left(\frac{1}{T_\odot}\right) M_\odot, \tag{5}$$

where m_1 and m_2 are the pulsar and companion mass in solar units, $s \equiv \sin i$ (i being the angle between the line of sight toward the pulsar and the right-handed normal

Table 1. *Selected parameters of binary pulsars*

(Most primary references not already quoted in the text may be found in Bhattacharya & van den Heuvel (1991). Parameters of PSR J2019+2425 are from unpublished work by the author and D. J. Nice.)

PSR	P/ms	$\log_{10}\dot{P}$	P_b/d	e	x/s	likely $\frac{m_2}{M_\odot}$
0021−72E	3.54	·	2.220	< 0.05	2.000	0.19
0021−72J	2.10	·	0.121	< 0.01	0.041	0.02
0655+64	195.67	−18.2	1.029	0.000008	4.126	0.81
0820+02	864.87	−16.0	1232.470	0.011868	162.147	0.23
1257+12[a]	6.22	−18.9	66.550	0.020	0.001312	1.2×10^{-5}
·	·	·	98.211	0.022	0.001414	1.0×10^{-5}
1259−63	47.76	·	≳ 1100	0.97	~ 3500	> 10
1310+18	33.16	·	255.840	< 0.005	84.170	0.36
1534+12	37.90	−17.6	0.421	0.273676	3.729	1.65[b]
1620−26	11.07	−18.1	191.443	0.02533	64.809	0.33
1639+36B	3.53	·	1.259	< 0.01	1.389	0.19
1744−24A	11.56	−19.7	0.076	< 0.0012	0.120	0.10
1802−07	23.10	−18.3	2.617	0.21202	3.920	0.36
1820−11	279.83	−14.9	357.762	0.79462	200.672	0.80
1831−00	520.95	−16.8	1.811	< 0.004	0.723	0.07
1855+09	5.36	−19.7	12.327	0.000022	9.231	0.29[b]
1913+16	59.03	−17.1	0.323	0.617131	2.342	1.08[b]
1953+29	6.13	−19.5	117.349	0.000330	31.413	0.21
1957+20	1.61	−19.8	0.382	< 0.00004	0.089	0.03
J2019+2425	3.93	−19.2	76.512	0.000111	38.768	0.37
2127+11C	30.53	−17.3	0.335	0.681411	2.520	1.15[b]
2303+46	1066.37	−15.2	12.340	0.658380	32.688	1.46[b]

[a] PSR 1257+12 appears to be orbited by two planet-sized masses.
[b] Better information on the masses is presented in table 2.

to the orbital plane), $T_\odot \equiv GM_\odot/c^3 = 4.925\,490\,947\times10^{-6}$ s, and G is the newtonian constant of gravity. To illustrate some distinguishing characteristics of the binary pulsars, and to provide a basis for further discussion, the mass functions for the listed objects except PSR 1257+12 (see below) are plotted as a function of orbital eccentricity in figure 5.

Obviously the mass function for a binary pulsar does not by itself yield independent values for m_1, m_2, or s. However, one can estimate a likely value for m_2 by assuming a pulsar mass, say $m_1 = 1.4M_\odot$, and the median value $|\cos i| = 0.5$. Values of m_2 computed in this way are listed in the final column of table 1. The true values of m_2 are unlikely to be grossly different from these guesses; better mass estimates cannot be obtained unless additional parameters are measured.

One of the pulsars in table 1, PSR 1257+12, is a special case: it participates in two keplerian orbits, each with a tiny mass function around $4\times10^{-16}M_\odot$ implying a planetary-sized companion (Wolszczan & Frail 1992). The remaining binary pulsars have orbital elements consistent with stellar-mass companions, and among these objects three additional categories can be distinguished. Fourteen have orbital eccentricities $e < 0.25$ and low-mass stellar companions thought to be degenerate dwarfs. Most of these have remarkably circular orbits: in fact, the only ones with eccentricities more than a few percent are located in globular clusters and have probably had their orbits perturbed by near collisions with other stars. Five of the

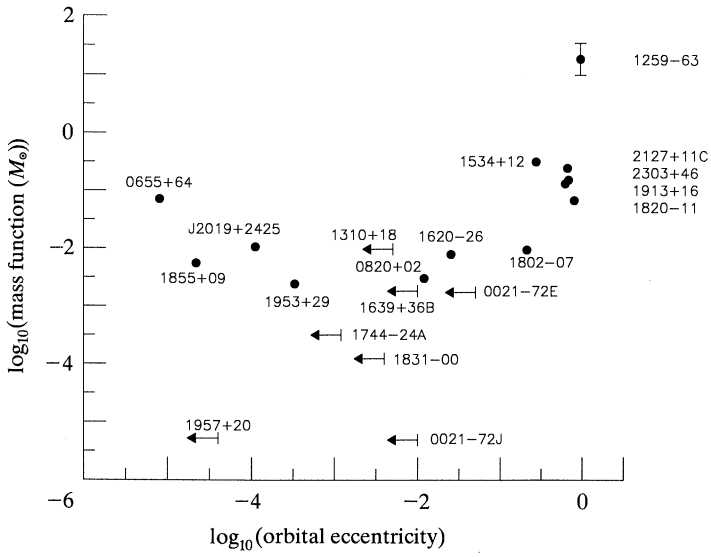

Figure 5. Mass functions of 20 binary pulsars, plotted as a function of orbital eccentricity.

binary systems have moderate-to-large values of both eccentricity and mass function. These are thought to be pairs of neutron stars, of which only one is a detectable pulsar. Their large orbital eccentricities are presumably caused by rapid mass loss accompanying the supernova explosion creating the second neutron star. Finally, at the high-mass end of the spectrum we find PSR 1259−63. This recently discovered pulsar moves in an extremely eccentric orbit around a massive Be star with a substantial stellar wind (Johnston *et al.* 1992).

(*b*) *General relativity as a tool*

If TOAs for a binary pulsar can be determined accurately enough to allow measurement of one or more post-keplerian (PK) parameters, further constraints on the system characteristics become available. Within a specified relativistic theory of gravity each measured PK parameter, together with the values of the keplerian orbital parameters, defines a curve in the m_1, m_2 plane. The measurement of any two PK parameters (say $\dot{\omega}$ and γ, or perhaps r and s) thus establishes uniquely the value of m_1, m_2, and through (5), $s \equiv \sin i$. The general relativistic equations for the five most significant PK parameters are as follows (see Damour & Deruelle 1986; Taylor & Weisberg 1989; Damour & Taylor 1992, and references therein):

$$\dot{\omega} = 3(P_b/2\pi)^{-\frac{5}{3}}(T_\odot M)^{\frac{2}{3}}(1-e^2)^{-1}, \tag{6}$$

$$\gamma = e(P_b/2\pi)^{\frac{1}{3}}T_\odot^{\frac{2}{3}}M^{-\frac{4}{3}}m_2(m_1+2m_2), \tag{7}$$

$$\dot{P}_b = -(192\pi/5)\,(P_b/2\pi)^{-\frac{5}{3}}(1+\tfrac{73}{24}e^2+\tfrac{37}{96}e^4)\,(1-e^2)^{-\frac{7}{2}}T_\odot^{\frac{5}{3}}\,m_1\,m_2\,M^{-\frac{1}{2}}, \tag{8}$$

$$r = T_\odot\, m_2, \tag{9}$$

$$s = x(P_b/2\pi)^{-\frac{2}{3}}T_\odot^{-\frac{1}{3}}M^{\frac{2}{3}}m_2^{-1}. \tag{10}$$

In these equations the masses m_1, m_2, and $M \equiv m_1 + m_2$ are all expressed in solar units.

The binary systems most likely to be sufficiently relativistic for measuring PK parameters are those which have large mass functions and orbital eccentricities, and which are astrophysically 'clean' so that the orbit is influenced only by the

Table 2. *Measured masses in binary pulsar systems*

(Numbers in parentheses represent uncertainties in the last digit. See text for references.)

PSR	$M/M_\odot$	$m_1/M_\odot$	$m_2/M_\odot$
1534+12	2.6781 (7)	1.34 (7)	1.34 (7)
1855+09	1.5 (2)	1.3 (2)	0.23 (2)
1913+16	2.82843 (2)	1.4411 (7)	1.3874 (7)
2127+11C	2.712 (5)	1.3 (2)	1.4 (2)
2303+46	2.9 (3)		

gravitational interaction between two compact masses. The large masses and eccentricities enhance the magnitudes of the relativistic effects, as may be seen in (6)–(9). Therefore PSRs 1534+12, 1820−11, 1913+16, 2127+11C, and 2303+46, clustered together in the upper right-hand portion of figure 5, would seem to be good candidate pulsars for measuring relativistic effects. In fact, measurements of three or more PK parameters have already been accomplished for PSRs 1534+12 and 1913+16, and their component masses are therefore well determined (see table 2 and further details in the next section). The parameters $\dot{\omega}$ and γ have been measured for PSR 2127+11C, and thus the masses in this system are known reasonably well. In this instance, however, the accuracy of γ is not yet very high. Consequently the total mass M, which can be determined from (6), is much better known than either m_1 or m_2 separately. The estimated values of M, m_1, and m_2 for PSR 2127+11C (S. Anderson, personal communication 1992) are listed in table 2.

The two remaining neutron-star binaries, PSRs 2303+46 and 1820−11, have much larger pulsar periods and orbital periods than the ones already discussed. For these objects the only PK parameter ever likely to be measurable is $\dot{\omega}$. Such measurements have been carried out successfully for PSR 2303+46 (Taylor & Dewey 1988; Bailes & Lyne 1990), and the resulting value of M is listed in table 2. Observations extended over a decade or so should be able to refine this value considerably (see §4).

In the most favourable circumstances, even low-mass binary pulsar systems with nearly circular orbits can yield useful PK parameters. The best present example of such a system is PSR 1855+09. Ryba & Taylor (1991) have shown that its orbital plane is nearly parallel to the line of sight, which magnifies the size and measurability of its Shapiro delay. The relevant observations are illustrated in figure 6, together with the fitted function $\Delta_S(r, s)$, in this case closely approximated by

$$\Delta_S = -2r \ln\left(1 - s\cos\left[2\pi(\phi - \phi_0)\right]\right), \tag{11}$$

where ϕ is the orbital phase in cycles and $\phi_0 = 0.4823$ is the phase of superior conjunction. The measured values of r and s yield the values of m_1 and m_2 listed in table 2 (Ryba & Taylor 1991). For this pulsar $\dot{\omega}$ is not measurable, and therefore M is known with no better precision than m_1 and m_2 separately.

(c) *Testing relativistic gravity*

If more than two post-keplerian parameters can be measured for a particular pulsar, the available information exceeds that required to determine the component masses and orbital inclination. The need for consistency then provides a means for explicit quantitative tests of relativistic gravity: one distinct test for each PK parameter beyond the first two. Note that the gravitational circumstances in a high-

PHILOSOPHICAL TRANSACTIONS OF THE ROYAL SOCIETY A MATHEMATICAL, PHYSICAL & ENGINEERING SCIENCES

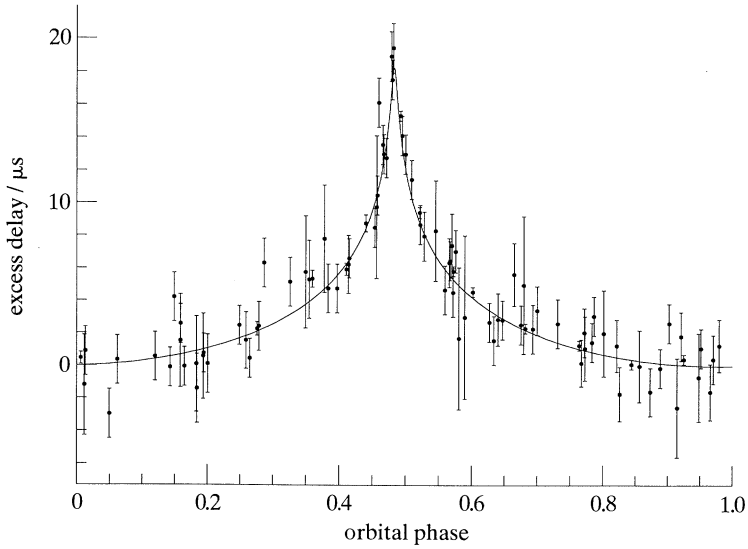

Figure 6. Measurement of the Shapiro delay in the PSR 1855+09 system. The plotted curve is the theoretical function for $\Delta_S(r, s)$, equation (11). The parameters r and s have been adjusted for best fit to the data. (After Ryba & Taylor 1991.)

mass binary pulsar system are considerably more extreme than the weak-field, slow-motion limit found throughout the Solar System. Two binary pulsars, PSRs 1913+16 and 1534+12, have now been timed long enough and accurately enough to yield three or more PK parameters. They provide significant tests of gravitation theories in conditions where strong-field and radiative effects are significant.

PSR 1913+16, the first binary pulsar to be discovered (Hulse & Taylor 1975), is the better known of the two. It has orbital period $P_b = 7.8$ h, eccentricity $e = 0.62$, and mass function $f_1 = 0.13\, M_\odot$; upon discovery it was immediately recognized as a likely candidate for testing general relatively, as well as for determining accurate neutron star masses. More than 4500 TOAs for this pulsar have been recorded at the Arecibo Observatory since 1974. Since 1981 their precision has been nearly constant, typically 15 μs in five-minute observations (see Taylor & Weisberg 1989, and references therein). With this accuracy and data span, the keplerian orbital parameters have been determined with fractional accuracies of a few parts per million or better. The PK parameters $\dot{\omega}$, γ, and $\dot{P}_b$ are determined to fractional accuracies of 4×10^{-6}, 7×10^{-4}, and 4×10^{-3}, respectively (see Taylor *et al.* 1992). It follows that the experiment can uniquely determine the stellar masses within any viable relativistic theory of gravity, and at the same time produce a test of the damping effects of gravitational radiation in that theory with an accuracy better than 0.5%.

The most recent experimental values for P_b, e, $\dot{\omega}$, and γ for the PSR 1913+16 system are listed at the top of table 3. These quantities and their covariances yield values for $\dot{P}_b^{GR}$, the predicted rate of period decay from gravitational radiation according to general relativity, and its uncertainty. The prediction is listed in table 1, followed by the observed period decay rate, $\dot{P}_b^{obs}$, and its experimental uncertainty. As shown by Damour & Taylor (1991), after gravitational radiation is accounted for there are no other plausible dissipative effects contributing more than a few parts in 10^5 of the total orbital period derivative. There is, however, a significant kinematic

PHILOSOPHICAL TRANSACTIONS OF THE ROYAL SOCIETY A MATHEMATICAL, PHYSICAL & ENGINEERING SCIENCES

Figure 7

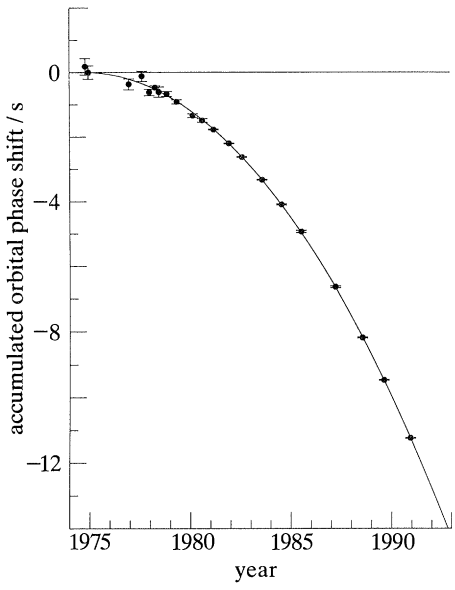

Figure 8

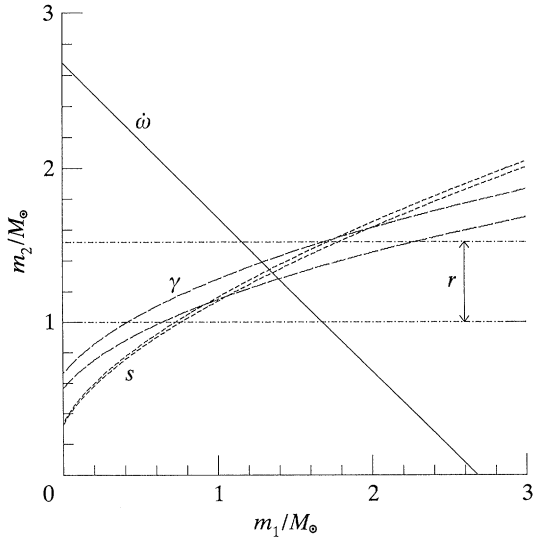

Figure 7. Filled circles represent measured shifts of the times of periastron passage of PSR 1913+16, relative to a non-dissipative model in which the orbital period remains fixed at its 1974.78 value. The most recent error bars, too small to see here, have lengths of approximately ± 0.01 s. The smooth curve illustrates the predicted damping from gravitational radiation, according to general relativity. (Observations carried out in collaboration with R. Hulse, L. Fowler, P. McCulloch, and J. Weisberg.)

Figure 8. Parametric curves corresponding to experimental constraints on the post-keplerian parameters $\dot{\omega}, \gamma, r$, and s for PSR 1534+12, according to general relativity. Pulsar and companion star masses $m_1 = m_2 = 1.34 \pm 0.07 M_\odot$ are consistent with all of the measurements. (Observations carried out in collaboration with A. Wolszczan.)

Table 3. *Observed and predicted parameters of the PSR 1913+16 system*

orbital period, P_b/s	27906.980 7807 ± 0.000 0009
orbital eccentricity, e	0.617 1309 ± 0.000 0006
rate of periastron advance, $\dot{\omega}$/(deg a^{-1})	4.226 628 ± 0.000 018
Einstein delay, γ/μs	4294 ± 3
predicted period decay, $\dot{P}_b^{GR}/10^{-12}$	−2.402 58 ± 0.000 04
observed period decay, $\dot{P}_b^{obs}/10^{-12}$	−2.425 ± 0.010
kinematic correction, $\dot{P}_b^{gal}/10^{-12}$	−0.017 ± 0.005
$(\dot{P}_b^{obs} - \dot{P}_b^{gal})/\dot{P}_b^{GR}$	1.002 ± 0.005

effect caused by acceleration of the Solar System and the PSR 1913+16 system in the galactic gravitational field. This effect is listed in table 3 as an additive correction, $\dot{P}_b^{gal}$. Its value depends on the size and rotation rate of the Galaxy, and on the pulsar distance and angular proper motion in the sky, all of which have been measured to adequate accuracy by means of other astronomical observations.

Figure 7 presents a comparison of the observed decay of the orbital period with the amount predicted by general relativity. (On the scale of this graph, the kinematic correction term $\dot{P}_b^{gal}$ is not visible.) Both table 3 and figure 7 show that the observations are in excellent accord with theoretical expectations. Indeed, the better-than-0.5% quantitative agreement is an impressive confirmation of Einstein's

PHILOSOPHICAL TRANSACTIONS OF THE ROYAL SOCIETY A MATHEMATICAL, PHYSICAL & ENGINEERING SCIENCES

theory, in a régime where gravitation theories have not previously been testable. This binary pulsar timing experiment provides direct confirmation that the gravitational interaction propagates at the finite velocity c, thereby creating a dissipative mechanism in an orbiting system, and that gravitational radiation must exist and must have a quadrupolar nature.

PSR 1534+12 was discovered just two years ago (Wolszczan 1990), and promises in many ways to yield results surpassing those available from PSR 1913+16. It has orbital period $P_b = 10.1$ h, eccentricity $e = 0.27$, and mass function $f_1 = 0.31 M_\odot$. Moreover, it has a stronger signal and narrower pulse shape than PSR 1913+16 (see figure 3); consequently the measurement uncertainties of its TOAs are considerably smaller, approximately 3 μs for five-minute observations. Results published by Taylor *et al.* (1992), based on slightly more than one year of data, include significant measurements of the PK parameters $\dot{\omega}$, γ, r, and s. Their links to the component masses through (6)–(10) are illustrated in figure 8. On the scale of this graph, the experimental uncertainty in $\dot{\omega}$ is negligible; for γ, r, and s, pairs of curves are used to illustrate the appropriate 1σ confidence intervals. All measured parameters of the PSR 1534+12 system are consistent (within general relativity) with masses $m_1 = m_2 = 1.34 \pm 0.07\, M_\odot$, and the theory thus passes a significant test under strong-field conditions. These results also provide useful constraints on other theories of gravity (Taylor *et al.* 1992), as will be further elaborated at this Discussion Meeting by Damour.

4. Future prospects

Damour & Taylor (1992) have carefully explored the potential measurabilities of PK parameters in binary pulsar systems, using PSRs 1913+16 and 1534+12 as explicit examples. They also published a series of graphs illustrating the measurabilities of PK parameters for 'generic' binary pulsars with a wide variety of orbital parameters. As an expository aid, I have now extended this work by simulating an explicit series of timing measurements for each of the 13 binary systems listed in table 4. The simulated data-sets are based on the orbital parameters listed in tables 1 and 2; if no pulsar mass is listed in table 2, the value $m_1 = 1.4 M_\odot$ was assumed. As in the earlier work (Damour & Taylor 1992), observations were assumed to have been made on a schedule of one observing session per month, for 10 years, with each session yielding 24 five-minute measurements. The assumed uncertainties of the five-minute TOAs are listed as the quantity σ_5 in table 4; they are consistent with uncertainties now actually achievable at Arecibo or other observatories.

For each of the 13 simulated data-sets, I computed the signal-to-noise ratios S (defined as the general relativistic values divided by the simulated measurement uncertainties) for the six PK parameters $\dot{\omega}, \gamma, \dot{P}_b, r, s$, and δ_θ. The number of significant decimal digits of each measurement is thus approximately $\log_{10}(1+S)$, and these values are listed in columns 3–8 of table 4. Note that for five binary systems, PSRs 0655+64, 0820+02, 1831−00, 1953+29, and J2019+2425, none of the PK parameters is expected to be measurable. These pulsars are low-mass, low-eccentricity systems (cf. figure 5 and table 1) that are intrinsically not very relativistic; there is little hope of measuring PK parameters for any of them unless, as for PSR 1855+09, the orbital inclination is close to $i = \frac{1}{2}\pi$. Similar circumstances apply for those binary systems listed in table 1 but not in table 4; all of them are expected to have negligible relativistic parameters and/or to be astrophysically

Table 4. *Simulated measurements of post-keplerian parameters*

(Each simulation assumed that 24 five-minute observations were made every month for 10 years, with uncertainties in TOAs given by σ_5.)

		number of measurable digits						
PSR	σ_5/μs	$\dot{\omega}$	γ	$\dot{P}_b$	r	s	δ_θ	$\log_{10}\lvert\dot{G}/G\rvert/a^{-1}$
0655+64	70	0	0	0	0	0.2	0	−10.6
0820+02	500	0	0	0	0	0	0	−8.1
1534+12	3	5.4	2.5	2.1	1.3	2.4	0.3	−12.7
1620−26	15	0.7	0	0	0.1	0.3	0	−10.1
1802−07	65	2.8	0.1	0	0	0.1	0	−10.1
1820−11	500	0.8	0	0	0	0	0	−8.8
1831−00	2000	0	0	0	0	0	0	−8.1
1855+09	3	0.1	0	0	1.4	3.6	0	−11.3
1913+16	15	4.9	2.8	2.5	0.1	0.6	0.1	−11.4
1953+29	30	0	0	0	0	0.1	0	−9.7
J2019+2425	15	0	0	0	0.1	0.4	0	−10.3
2127+11C	100	4.4	2.2	2.0	0.1	0.2	0	−10.7
2303+46	2000	1.6	0	0	0	0	0	−9.5
scaling law[a]		1	2	2	0	0	2	2

[a] Signal-to-noise ratios of the various quantities scale as the total data span to the specified power.

complicated systems so that clean separation of such effects would be impossible. PSRs 1802−07 and 2303+46 should yield clean and accurate measurements of $\dot{\omega}$, and PSRs 1620−26 and 1820−11 should provide $\approx 20\%$ measurements; hence, with diligence the total masses of these systems can be determined to useful accuracy.

The remaining pulsars in table 4, PSRs 1534+12, 1913+16, and 2127+11C, are high-mass, high-eccentricity, neutron star binaries with orbital periods less than 12 h. In the 10-year simulations these pulsars yielded five, four and three measurable PK parameters, respectively, and in most cases the predicted precisions are quite high. For PSR 1534+12, in particular, four PK parameters should be measurable to 1% or better in 10 years, and r should be measurable to about 6%. Furthermore, by applying the scaling law listed in the bottom line of the table we see that even δ_θ might be measurable for this pulsar with 20–30 years of observations. For PSR 1913+16 the simulations essentially reproduce the present state of the real observations: $\dot{\omega}$, γ, and $\dot{P}_b$ are accurately measurable, but s and especially r will be difficult to measure without improved data. (As shown by Damour & Taylor (1992), these parameters will become much more easily measurable around the year 2017, when the longitude of periastron is more favourable.) PSR 2127+11C will yield improved measurements of $\dot{\omega}$ and γ, as well as a good value for $\dot{P}_b$, with a 10-year data span.

A summary of the present status and the foreseeably achievable results for $\dot{\omega}$ and $\dot{P}_b$ is shown for 10 well-studied pulsars in figure 9. Here the pulsars have been ranked from left to right in order of the measured or predicted values of $\dot{\omega}$. The vertical scale is logarithmic, with values of $\dot{\omega}$ plotted above the pulsar names and inverse orbital-decay timescales plotted below. Filled circles represent real measurements, and downward pointing arrows are experimental upper limits. The excellent near-term prospects for measuring $\dot{\omega}$ for PSR 1802−07, and $\dot{P}_b$ for PSRs 2127+11C and 1534+12, are evident in the figure. On the other hand, it is clear that these

PHILOSOPHICAL TRANSACTIONS OF THE ROYAL SOCIETY A MATHEMATICAL, PHYSICAL & ENGINEERING SCIENCES

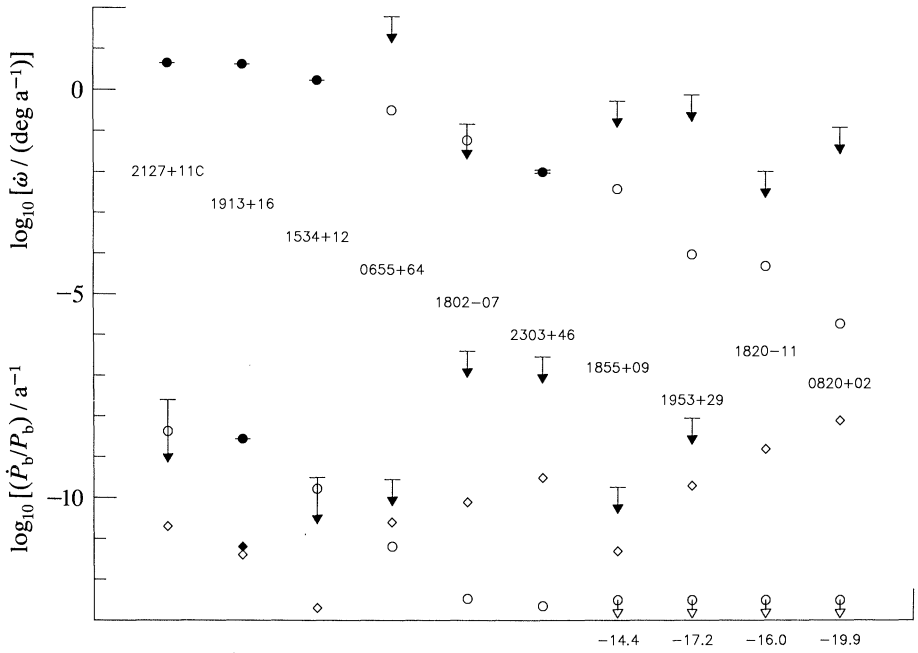

Figure 9. Observed and simulated measurements of $\dot{\omega}$ (symbols above the pulsar names) and $\dot{P}_b/P_b$ (symbols below the names) for 10 binary pulsars. The pulsars are arranged in decreasing order of the measured or predicted magnitudes of $\dot{\omega}$. Filled circles with very small error bars represent real measurements, and horizontal bars with downward pointing arrows give presently available upper limits. Open circles give the approximate predicted values for unmeasured quantities. Open diamonds correspond to phenomenological limits on $|\dot{G}/G| = |\delta\dot{P}_b/2P_b|$ that could be obtained with 10 years of monthly timing observations at present levels of accuracy, and the filled diamond indicates the present limit from observations of PSR 1913+16.

parameters will not be measurable in the foreseeable future for most of the other pulsars. Most of the orbital-decay timescales, for example, far exceed the Hubble time and will not produce observable consequences over human lifetimes.

Diamond shaped open symbols near the bottom of figure 9 correspond to numbers quoted in the last column of table 4, and indicate the phenomenological limits on $|\dot{G}/G| = |\delta\dot{P}_b/2P_b|$ that should be achievable with 10-year data spans. (G is Newton's constant, and $\delta\dot{P}_b$ the unexplained excess or uncertainty in measuring $\dot{P}_b$; for details see Damour *et al.* 1988). The best existing limits on $\dot{G}/G$, including one indicated by the filled diamond in figure 9, based on observations of PSR 1913+16, lie between 10^{-11} and $10^{-12}\,a^{-1}$. A comparable limit appears achievable with data from PSR 1855+09, and possibly 0655+64, and for these pulsars the results will not be complicated by questions about the equation of state of the companion star (see Nordtvedt 1990). Better still, however, a much improved limit approaching $10^{-13}\,a^{-1}$ appears achievable with timing observations of PSR 1534+12.

For several reasons related to topics in this and earlier sections, it is clear that long-term programmes of timing recycled pulsars are very desirable: there appear to be few opportunities as attractive for experimental input on the fundamental nature of gravity and its cosmological connections. Note that several of the scaling laws listed at the bottom of table 4 are especially favourable for long-term studies. For most pulsars, measurements of γ, $\dot{P}_b$, δ_θ, and $\dot{G}/G$ should be 10 times more accurate with three decades of observations as with one, and 100 times more accurate within

PHILOSOPHICAL TRANSACTIONS OF THE ROYAL SOCIETY A MATHEMATICAL, PHYSICAL & ENGINEERING SCIENCES

a century. Thus it behoves us to make careful observations and to document them well, so that our results can be of quantitative use to future generations of investigators.

I am indebted to numerous colleagues including T. Damour, M. Davis, R. Dewey, L. Fowler, R. Hulse, P. McCulloch, D. Nice, L. Rawley, M. Ryba, D. Segelstein, D. Stinebring, G. Stokes, S. Thorsett, A. Vázquez, J. Weisberg, and A. Wolszczan for significant contributions to work described in this paper. Much of the research was supported by the U.S. National Science Foundation.

Appendix A. Determining pulse times of arrival

The applications of pulsar timing discussed in this paper depend crucially on the precision of measuring pulse times of arrival, so it is important to make the best possible use of all information in the data. Let us assume that observed and standard profiles, $p(t)$ and $s(t)$, have been obtained as described in §2a: the profiles are sampled and recorded at equally spaced intervals of time, $t_j = j\Delta t$, $j = 0, 1, \ldots, N-1$, with $P = N\Delta t$. Before sampling, the detected signals will have been low-pass filtered at a cutoff frequency $f_c \leqslant (2\Delta t)^{-1}$. To avoid filtering out useful data, Δt is chosen small enough that f_c can exceed the highest frequencies significantly present in the data. (Obviously what is 'significant' will depend on the available signal-to-noise ratio.) If the foregoing criteria are met, the finite sampling theorem (Bracewell 1965) ensures that all potentially available information is fully and unambiguously contained in the discretely sampled values $p_j = p(t_j)$.

If $p(t)$ is equal to a shifted and scaled replica of $s(t)$ plus random noise, as defined in (1), their Fourier transforms are also related in a simple way. Discrete Fourier transforms of the two profiles can be written as

$$P_k \exp(\mathrm{i}\theta_k) = \sum_{j=0}^{N-1} p_j \, \mathrm{e}^{\mathrm{i}2\pi jk/N}, \tag{A 1}$$

$$S_k \exp(\mathrm{i}\phi_k) = \sum_{j=0}^{N-1} s_j \, \mathrm{e}^{\mathrm{i}2\pi jk/N}, \tag{A 2}$$

where the frequency index k runs from 0 to $N-1$. Thus, the real quantities P_k and S_k are the amplitudes of the complex Fourier coefficients, and θ_k and ϕ_k are the phases. Linearity of the transform relationship implies that

$$P_k \exp(\mathrm{i}\theta_k) = aN + bS_k \exp[\mathrm{i}(\phi_k + k\tau)] + G_k, \quad k = 0, \ldots, \quad (N-1), \tag{A 3}$$

where G_k represents random noise equal to the Fourier transform of the sampled noise in the time-domain profile, $g(t_j)$. Note that the bias a and scale factor b assume similar roles in the time and frequency domain (cf. equation (1)). As a consequence of the 'shift theorem' (Bracewell 1965), the time offset τ appears in the frequency domain as the slope of a linear ramp, $k\tau$, added to the phases of the standard profile's Fourier coefficients. After the transforms have been computed, the value of a can be obtained immediately from the relation

$$a = (P_0 - bS_0)/N. \tag{A 4}$$

The desired pulse time of arrival τ, as well as the gain factor b, can be obtained by minimising the goodness-of-fit statistic

$$\chi^2(b, \tau) = \sum_{k=1}^{N/2} \left| \frac{P_k - bS_k \exp[\mathrm{i}(\phi_k - \theta_k + k\tau)]}{\sigma_k} \right|^2. \tag{A 5}$$

In this equation σ_k is the root-to-mean-square amplitude of the noise at frequency k, and presumably the anti-aliasing low-pass filter will make the σ_ks fall off somewhat at larger values of k. In practice, however, this subtlety is usually unimportant since the amplitudes P_k and S_k decrease even faster than σ_k. Owing to inherent symmetries in the transforms, the limits of summation in (A 5) can be taken as 1 to $\frac{1}{2}N$, rather than 0 to $N-1$. For convenience of notation, in the remaining equations the summation limits have been omitted and the σ_ks treated as constant.

By replacing the complex exponential in (A 5) with trigonometric equivalents and expanding the indicated squared modulus, one obtains a more convenient expression for χ^2, namely

$$\chi^2 = \sigma^{-2}\Sigma\,(P_k^2 + b^2 S_k^2) - 2b\sigma^{-2}\Sigma\,P_k S_k \cos\,(\phi_k - \theta_k + k\tau). \tag{A 6}$$

At the global minimum of the two-dimensional function $\chi^2(\tau, b)$, its derivatives with respect to τ and b must vanish. This requirement yields two equations in the two unknowns, namely

$$\frac{\partial\chi^2}{\partial\tau} = \frac{2b}{\sigma^2}\Sigma\,kP_k S_k \sin\,(\phi_k - \theta_k + k\tau) = 0, \tag{A 7}$$

$$\frac{\partial\chi^2}{\partial b} = \frac{2b}{\sigma^2}\Sigma\,S_k^2 - \frac{2}{\sigma^2}\Sigma\,P_k S_k \cos\,(\phi_k - k\tau) = 0. \tag{A 8}$$

Equation (A 7) can be solved for τ by a straightforward iterative procedure such as Brent's method (see, for example, Press *et al.* 1986). Equation (A 8) then yields

$$b = \Sigma\,P_k S_k \cos\,(\phi_k - \theta_k + k\tau)/\Sigma\,S_k^2. \tag{A 9}$$

Uncertainties in the estimated values of τ and b may be found by approximating χ^2 near its minimum by the leading terms of a Taylor series, and determining the excursions of b or τ required to increase the value of χ^2 by 1. This procedure leads to

$$\sigma_\tau^2 = \left(\frac{\partial^2\chi^2}{\partial\tau^2}\right)^{-1} = \frac{\sigma^2}{2b\,\Sigma\,k^2 P_k S_k \cos\,(\phi_k - \theta_k + k\tau)}, \tag{A 10}$$

$$\sigma_b^2 = \left(\frac{\partial^2\chi^2}{\partial b^2}\right)^{-1} = \frac{\sigma^2}{2\,\Sigma\,S_k^2}. \tag{A 11}$$

Notice that the data sampling interval, $\Delta t = P/N$, appears nowhere in (A 1)–(A 10). Our formalism for fitting TOAs in the Fourier transform domain places no limits on accuracy expressed as a fraction of Δt. In contrast, experience has shown that time-domain methods widely in use for determining TOAs do not readily produce arrival-time accuracies smaller than about $0.1\Delta t$ (see, for example, Rawley 1986).

References

Alpar, M. A., Cheng, A. F., Ruderman, M. A. & Shaham, J. 1982 A new class of radio pulsars. *Nature, Lond.* **300**, 728–730.

Bailes, M. & Lyne, A. G. 1990 The mass of the PSR 2303+46 system. *Mon. Not. R. astr. Soc.* **246**, 15P–17P.

Bertotti, B., Carr, B. J. & Rees, M. J. 1983 Limits from the timing of pulsars on the cosmic gravitational wave background. *Mon. Not. R. astr. Soc.* **203**, 945–954.

Bhattacharya, D. & van den Heuvel, E. P. J. 1991 The formation and evolution of binary and millisecond radio pulsars. *Phys. Rep.* **203**, 1–124.

Blandford, R. D., Narayan, R. & Romani, R. W. 1984 Arrival-time analysis for a millisecond pulsar. *J. Astrophys. Astr.* **5**, 369–388.

Bracewell, R. 1965 *The Fourier transform and its applications*. New York: McGraw-Hill.

Damour, T. & Deruelle, N. 1985 General relativistic celestial mechanics of binary systems. I. The post-Newtonian motion. *Ann. Inst. H. Poincaré* (*Physique Théorique*) **43**, 107–132.

Damour, T. & Deruelle, N. 1986 General relativistic celestial mechanics of binary systems. II. The post-Newtonian timing formula. *Ann. Inst. H. Poincaré* (*Physique Théorique*) **44**, 263–292.

Damour, T., Gibbons, G. & Taylor, J. H. 1988 Upper limit on rate of change of the gravitational constant. *Phys. Rev. Lett.* **61**, 1151–1154.

Damour, T. & Taylor, J. H. 1991 On the orbital period change of the binary pulsar PSR 1913+16. *Astrophys. J.* **366**, 501–511.

Damour, T. & Taylor, J. H. 1992 Strong-field tests of relativistic gravity and binary pulsars. *Phys. Rev.* D**45**, 1840–1868.

Hewish, A., Bell, S. J., Pilkington, J. D. H., Scott, P. F. & Collins, R. A. 1968 Observation of a rapidly pulsating radio source. *Nature, Lond.* **217**, 709–713.

Hulse, R. A. & Taylor, J. H. 1975 Discovery of a pulsar in a binary system. *Astrophys. J. Lett.* **195**, L51–L54.

Johnston, S., Manchester, R. N., Lyne, A. G., Bailes, M., Kaspi, V., Guojun, Q. & D'Amico, N. 1992 PSR 1259−63: A binary radio pulsar with a Be star companion. *Astrophys. J. Lett.* **387**, L37–L41.

Manchester, R. N. & Peters, W. L. 1972 Pulsar parameters from timing observations. *Astrophys. J.* **173**, 221–226.

Manchester, R. N. & Taylor, J. H. 1977 *Pulsars*, ch. 6. San Francisco: Freeman.

Nordtvedt, K. 1990 $\dot{G}/G$ and a cosmological acceleration of gravitationally compact bodies. *Phys. Rev. Lett.* **65**, 953–956.

Press, W. H., Flannery, B. P., Teukolsky, S. A. & Vetterling, W. T. 1986 *Numerical recipes: the art of scientific computing*. Cambridge University Press.

Rawley, L. A. 1986 Timing millisecond pulsars. Ph.D. thesis, Princeton University.

Rawley, L. A., Taylor, J. H. & Davis, M. M. 1988 Fundamental astrometry and millisecond pulsars. *Astrophys. J.* **326**, 947–953.

Rawley, L. A., Taylor, J. H., Davis, M. M. & Allan, D. W. 1987 Millisecond pulsar PSR 1937+21: a highly stable clock. *Science, Wash.* **238**, 761–765.

Ryba, M. F. & Taylor, J. H. 1991 High precision timing of millisecond pulsars. I. Astrometry and masses of the PSR 1855+09 system. *Astrophys. J.* **371**, 739–748.

Stinebring, D. R., Kaspi, V. M., Nice, D. J., Ryba, M. F., Taylor, J. H., Thorsett, S. E. & Hankins, T. H. 1992 A flexible data acquisition system for timing pulsars. *Rev. sci. Instrum.* (In the press.)

Stinebring, D. R., Ryba, M. F., Taylor, J. H. & Romani, R. W. 1990 Cosmic gravitational-wave background: limits from millisecond pulsar timing. *Phys. Rev. Lett.* **65**, 285–288.

Taylor, J. H. 1991 Millisecond pulsars: nature's most stable clocks. *Proc. IEEE* **79**, 1054–1062.

Taylor, J. H. & Dewey, R. J. 1988 Improved parameters for four binary pulsars. *Astrophys. J.* **332**, 770–776.

Taylor, J. H. & Weisberg, J. M. 1989 Further experimental tests of relativistic gravity using the binary pulsar PSR 1913+16. *Astrophys. J.* **345**, 434–450.

Taylor, J. H., Wolszczan, A., Damour, T. & Weisberg, J. M. 1992 Experimental constraints on strong-field relativistic gravity. *Nature, Lond.* **355**, 132–136.

Wolszczan, A. 1991 A nearby 37.9 ms radio pulsar in a relativistic binary system. *Nature, Lond.* **350**, 688–690.

Wolszczan, A. & Frail, D. 1992 A planetary system around the millisecond pulsar PSR 1257+12. *Nature, Lond.* **355**, 145–146.

PHILOSOPHICAL TRANSACTIONS OF THE ROYAL SOCIETY A MATHEMATICAL, PHYSICAL & ENGINEERING SCIENCES